THE JOURNAL OF PHYSICAL CHEMISTRY A

Article

Cite This: J. Phys. Chem. A 2017, 121, 9320−9329

pubs.acs.org/JPCA

Removal of Pb(II) Ion Using PAMAM Dendrimer Grafted Graphene and Graphene Oxide Surfaces: A Molecular Dynamics Study

Anitha Kommu, Vasumathi Velachi, Maria Natália D. S. Cordeiro, and Jayant K. Singh*

Department of Chemical Engineering, Indian Institute of Technology Kanpur, Kanpur-208016, India

LAQV@REQUIMTE/Department of Chemistry and Biochemistry, Faculty of Sciences, University of Porto, 4169-007 Porto, Portugal

Supporting Information

ABSTRACT: The dendrimer polyamidoamine (PAMAM) has been widely applied in environmental applications as adsorbents for wastewater treatment. In this work, molecular dynamics simulations are conducted to understand the effect of dendrimer grafted graphene and graphene oxide on the structural and dynamical properties of the Pb^{2+} ion. The adsorption capacity of the metal ion is improved significantly, over 60%, using carboxyl terminal groups of a dendrimer molecule grafted on a graphene oxide surface. We examine the self-diffusion coefficient and residence time of Pb^{2+} ion near graphene and graphene oxide surfaces grafted with PAMAM dendrimers using terminal groups, $-COO^-$ and $-OH$. Further, the potential of mean force is analyzed to understand the role of different surface groups in enhancing the adsorption of the metal ion.

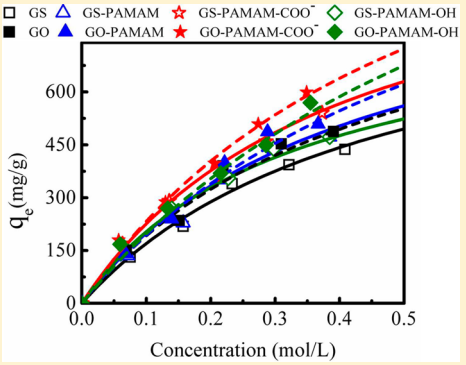

1. INTRODUCTION

The water pollution due to the indiscriminate disposal of heavy metal ions and their toxicity is one of the biggest issues faced by a developing country. Wastewater from many industries such as metallurgical, mining, chemical manufacturing, battery, printing, and paper industries, etc., contains various types of toxic pollutants[1−7] including heavy metals. The heavy metals are not biodegradable and tend to accumulate in living organisms. Many metal ions like cadmium, lead, arsenic, chromium, and mercury are known to be carcinogenic agents, and thus are a serious threat to human beings and animals.[7,8] Some heavy metals like iron, zinc, cobalt, copper, manganese, etc., however, are essential to life and play an irreplaceable role in the human metabolic system like the functioning of critical enzyme sites, but they can harm the organism to an excessive level.[9] Therefore, it is necessary to eliminate these toxic heavy metal ions from wastewater before they are released into the environment.

Many conventional techniques such as chemical precipitation,[10] ion-exchange,[11] adsorption,[12] and membrane filtration technologies,[13,14] etc., have been used for the removal of heavy metal ions. However, these techniques have their inherent advantages and limitations. An adsorption based technique, on the other hand, is considered to be one of the simplest and most attractive methods for the removal of heavy metal ions and organic pollutants. Several adsorbents have been studied for adsorption of metal ions such as clay minerals, oxides, and carbon materials.[15−17] However, these adsorbents suffer from low adsorption capacities or removal efficiencies of metal ions.

In recent years, various promising novel materials have been developed which have a wide variety of applications. For example, carbon nanotubes,[18,19] carbon nanotube based material composites,[20] and graphene[21−23] have shown potential for the removal of hazardous pollutants from aqueous solutions, with high adsorption capacity. In particular, graphene and graphene composites have been studied as an adsorbent for removing heavy metal ions from aqueous streams.[22,24−31] A reduced graphene oxide composite exhibited a highly selective removal capacity for Hg^{2+} from wastewater.[22] In another work, graphene oxide aerogels are being used as an effective adsorbent for removal of Cu^{2+} from wastewater.[25] In addition, various molecular simulations studies reveal an important role for terminal groups on graphene based materials for enhanced removal of metal ions from aqueous streams.[32,33]

Polyamidoamine dendrimers (PAMAMs) are frequently studied due to their large amount of terminal functional groups.[34,35] PAMAM dendrimers are much larger and more versatile with regard to their variety of terminal groups, including amino, carboxylic, and hydroxyl groups. The grafted graphene oxide with dendrimers (GO-PAMAM) has shown a high adsorption capacity of heavy metal ions of ∼1.0 mmol/g.[36] Recent experimental work of Zhang et al.[37] explored using GO-PAMAM adsorbent to remove heavy metal ions from aqueous solutions. The maximum adsorption capacity of GO-PAMAM for Pb^{2+} was reported to be 568 mg/g, which is higher than that for other metal ions.[37] However, not much is known about the molecular interaction of ions with PAMAM dendrimers. This work investigates the molecular mechanisms involved in the

Received: October 2, 2017
Revised: November 15, 2017
Published: November 16, 2017

DOI: 10.1021/acs.jpca.7b09766
J. Phys. Chem. A 2017, 121, 9320−9329

adsorption of metal ions on the graphene, graphene oxide, and polyamidoamine (PAMAM) dendrimers with different terminal group grafted graphene and graphene oxide surfaces. In particular, we present a computational study of the metal ion adsorption behavior on the graphene and graphene oxide modified surfaces. The rest of the article is organized as follows. Section 2 presents the simulation methods and details. Results and discussion are presented in section 3, and finally, conclusions are given in section 4.

2. MODELS AND METHODS

In this work, using the base materials as listed in Table 1, eight different surfaces are generated, viz., graphene (GS), GS-PAMAM, GS-PAMAM-COO$^-$, GS-PAMAM-OH, graphene oxide (GO), GO-PAMAM, GO-PAMAM-COO$^-$, and GO-PAMAM-OH. The PAMAM dendrimer considered in this work is of the G3 generation. Using VMD software, GS of 71 Å × 71 Å sheet was built. For the atomistic GO model, we construct hydroxyl and epoxy groups functionalized on the basal plane. The epoxy and hydroxyl groups are randomly grafted to the carbon atoms on a 71 Å × 71 Å graphene basal plane (see Figure 1a). The carboxyl groups are also attached to the carbon atoms on the edges randomly (see Figure 1a). Using dendrimer builder toolkit (DBT), a PAMAM dendrimer of generation 3 is modeled. We have made a covalent bond between the GS/GO and the dendrimer by using the AMBER LEAP module.[38] The mentioned GS/GO-dendrimer covalent bond creates considerable chemical environmental changes on the core atoms of dendrimer and hybridization of carbon atoms of GS/GO. Hence, the atomic charges for the core atoms of the dendrimer are recalculated by using the Maingi et al.[39] scheme. In this scheme, the structure (for instant a segment of graphene sheet with core atoms of dendrimer) is optimized using GAUSSIAN03[40] with the HF/6-31G(d) basis set. The electrostatic potential (ESP) method is used for charge calculation during optimization. Now the charges of the carbon atom of GS/GO attached to the dendrimer and the core atoms are calculated using the restrained electrostatic potential (RESP) fitting method as implemented in the "antechamber" module of AMBER by giving the optimized ESP charges as an input file to the antechamber execution. Using the same scheme, the atomic charges of (i) various terminal group atoms of dendrimer, and (ii) the carbon atoms of GO attached to the functional groups such carboxyl, hydroxyl, and epoxy, and these functional group atoms are calculated. The dendrimer grafted on the GO and GS structures are solvated with water filled cubic box of edge length 150 Å. Solvated structures are energy minimized followed by the NPT MD simulations about 50 ns. An initial system for a metal ion adsorption study is generated by taking the above equilibrated structures of dendrimer grafted on the GO and GS surfaces (adsorbent) that are solvated in an aqueous concentration of $Pb(NO_3)_2$ ionic salts. An illustration of such a system is shown in Figure 1. The carboxyl groups are also attached to the carbon atoms on the edges randomly (see Figure 1a). The TIP3P model[41] is used to model water−water interaction, and OPLS (optimized potential for liquid simulation) parameters are used for metal ions, and graphene, and different terminal groups of the PAMAM dendrimer.[42−44] The Tummala et al.[45] and Shih et al.[46] reported force field is used for all sp^2 carbon atoms of the GO sheet. For oxidized regions in the atomistic GO model, we construct carboxyl-, hydroxyl-, and epoxy-functionalized graphene on the sheet such that n_O/n_C = 15%. The carbon atoms in the GS and GO surfaces are modeled as uncharged and are kept rigid.

Table 1. Summary of the Materials Considered in This Work

material	description
GS	graphene sheet
GO	graphene oxide
PAMAM	dendrimer with NH_2 terminal groups
PAMAM-COO$^-$	dendrimer with COO$^-$ terminal groups
PAMAM-OH	dendrimer with OH terminal groups

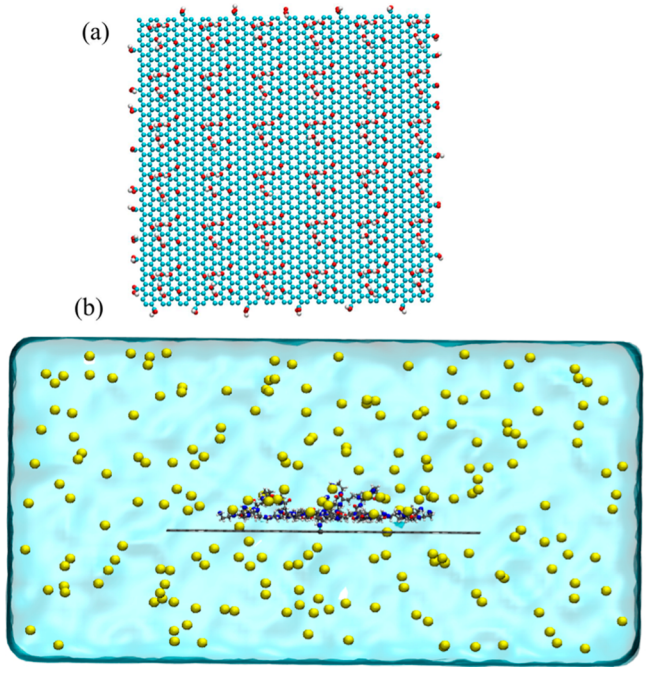

Figure 1. (a) Graphene oxide (GO) functionalized with hydroxyl, epoxy, and carboxyl groups. (b) Representative simulations system with the 0.1 M Pb^{2+} ion concentration and a GO-PAMAM surface. Gray color represents the GS; cyan, red, blue, and white colors represent the carbon atoms of PAMAM dendrimer, oxygen atoms of functional groups and PAMAM, nitrogen atoms of PAMAM, and hydrogen atoms of functional groups and PAMAM. Water is represented as the light blue surface, with nitrate ions represented as green and pink, and metal ions are shown in yellow.

The nonbonded interactions are described by the following equation.

$$U_{\text{nonbond}} = 4\varepsilon_{ij}\left[\left(\frac{\sigma_{ij}}{r_{ij}}\right)^{12} - \left(\frac{\sigma_{ij}}{r_{ij}}\right)^{6}\right] + \frac{q_i q_j}{4\pi\varepsilon_0 r_{ij}} \quad (1)$$

Here, ε_{ij} and σ_{ij} are the energy and length parameters of Lennard-Jones potential, respectively. The charges on the atoms i and j are represented by q_i, q_j, respectively, and r_{ij} denotes center to center distance. Here, ε_0 denotes the dielectric permittivity constant.

All the stretching and bending interactions are represented by harmonic potentials:

$$U_{\text{bond}} = \frac{1}{2}k_r(r - r_{\text{eq}})^2 \qquad U_{\text{angle}} = \frac{1}{2}k_\theta(\theta - \theta_{\text{eq}})^2 \quad (2)$$

Cross interaction parameters of unlike pairs of i and j particles are calculated by using Lorentz−Berthelot mixing rules.

DOI: 10.1021/acs.jpca.7b09766
J. Phys. Chem. A 2017, 121, 9320−9329

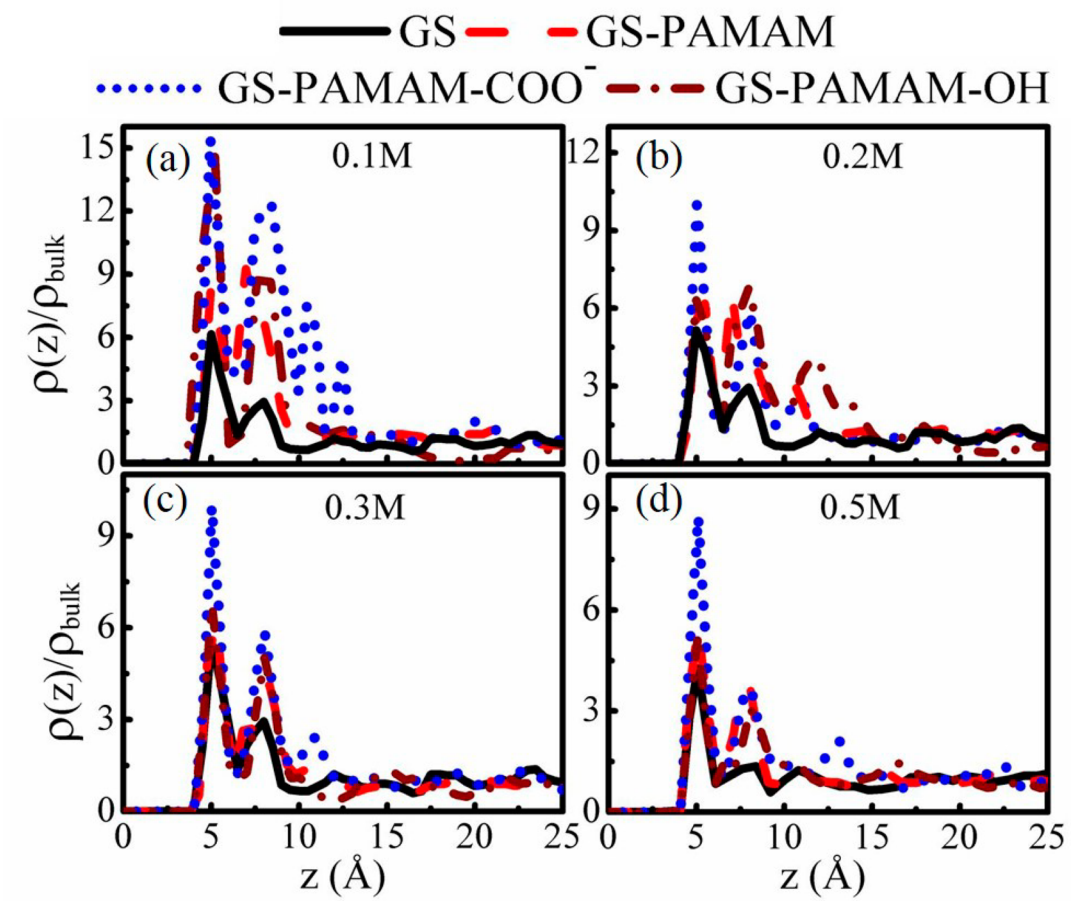

Figure 2. Normalized density profiles of Pb^{2+} from the surfaces (GS, GS-PAMAM, GS-PAMAM-COO^-, and GS-PAMAM-OH) at (a) 0.1 M, (b) 0.2 M, (c) 0.3 M, and (d) 0.5 M concentrations.

All MD simulations are carried out using the LAMMPS package.[47] Independent simulations are performed for eight different surfaces, solvated in five different concentrations (0.1, 0.2, 0.3, 0.4, and 0.5 M) for metal ion using their nitrate salt $Pb(NO_3)_2$ in an aqueous medium. A representative snapshot is shown in Figure 1b. An orthogonal simulation box (133.0 × 133.0 × 73.0 $Å^3$) is used containing the surface aligned along the *z*-axis. Subsequently, water (42 000) molecules and metal ions are added to the simulation box with the help of the Packmol program.[48] Periodic boundary conditions are applied in all directions. Long-range electrostatic interactions are accounted for using the particle−particle particle−mesh (PPPM) technique as implemented in LAMMPS. A cut off distance of 10 Å is used for the nonbonded interactions. A time step of 1.0 fs is used, and trajectories of the simulations are collected for every 10 ps for analysis. The simulation system is first equilibrated using a constant pressure and temperature (NPT) ensemble at 298 K and 1 atm for 1 ns. The temperature and pressure of the system are maintained using the Nosé−Hoover thermostat and barostat.[49,50] Further, we have used the equilibrium configurations from NPT simulations, of Pb^{2+} metal ion systems, to perform 50 ns constant volume and temperature (NVT) ensemble simulations at 298 K using a Nosé−Hoover thermostat. The trajectories of the system obtained from NVT simulations are used to calculate the adsorption capacity of ions on eight different surfaces.

The normalized radial density profiles ($\rho(z)/\rho_{bulk}$) of Pb^{2+} metal ions are calculated for five different concentrations. The occupation time distribution function of the metal ion is calculated using the time correlation function $R(t)$ as shown in eq 3. The residence time (τ_s) is evaluated by fitting an exponential form, as shown in eq 4, to the $R(t)$ values.

$$R(t) = \frac{\langle \sum_{i=1}^{N} \theta_i(t_0)\theta_i(t - t_0)\rangle}{\langle \sum_{i=1}^{N} \theta_i(t_0)\theta_i(t_0)\rangle} \tag{3}$$

$$R(t) = A \exp[-(t/\tau_s)] \tag{4}$$

The diffusion coefficients of metal ions are calculated from mean square displacement (MSD) using eqs 5 and 6.

$$\mathrm{MSD}(t) = \frac{1}{N}\sum_{i=1}^{N} (|r_i(t + \Delta t) - r_i(t)|)^2 \tag{5}$$

$$D = \frac{1}{4}\lim_{t\to\infty} \frac{\mathrm{d}}{\mathrm{d}t}(\mathrm{MSD}) \tag{6}$$

Here, $r_i(t)$ is the vector position of the atom "*i*" at time "*t*". *N* is the number of atoms of the divalent metal ions.

The nature of adsorption of metal ions on surfaces is described using the Langmuir isotherm:

$$q_e = \frac{q_{max} KC}{1 + KC} \tag{7}$$

Here q_e is the amount of metal ion adsorbed per unit mass of adsorbent (mg/g). The q_{max} (mg/g) is the maximum amount of metal ion adsorbed, and *K* is constant. The concentration (*C*,

DOI: 10.1021/acs.jpca.7b09766
J. Phys. Chem. A 2017, 121, 9320−9329

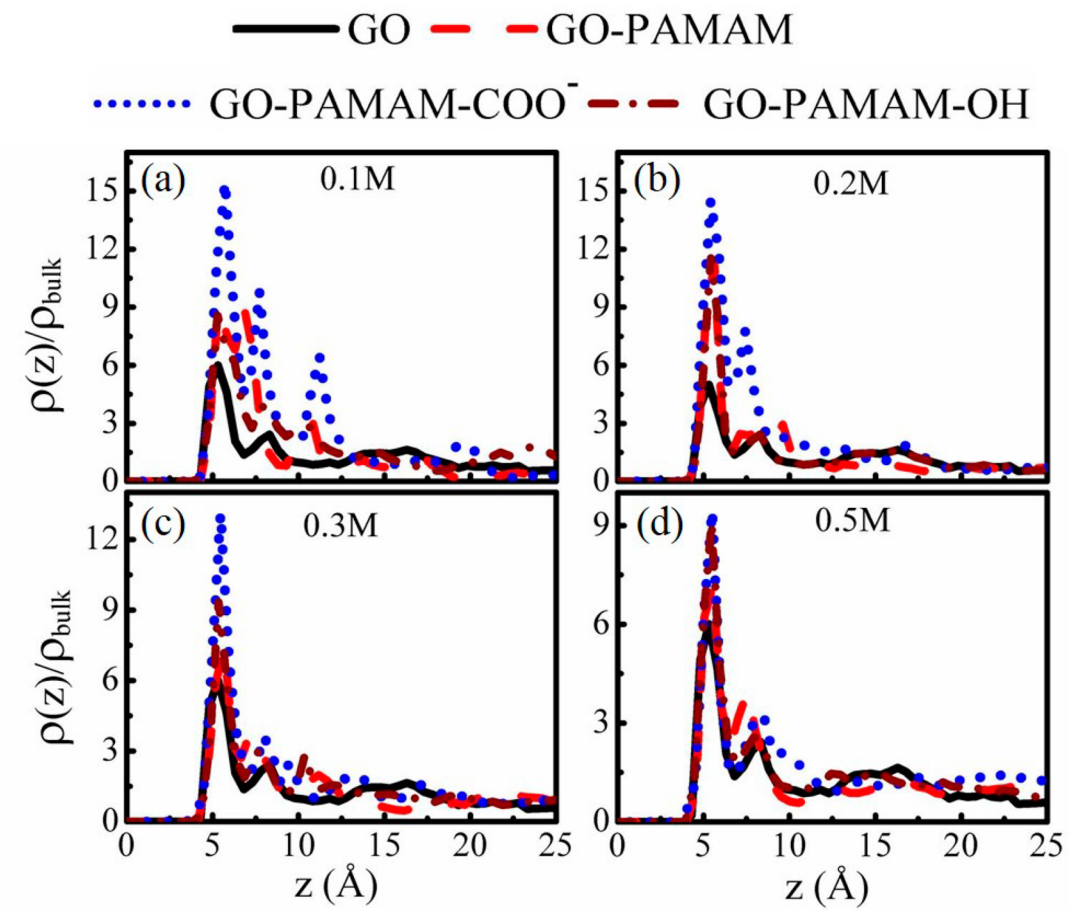

Figure 3. Normalized density profiles of Pb^{2+} from the surfaces (GO, GO-PAMAM, GO-PAMAM-COO^-, and GO-PAMAM-OH) at (a) 0.1 M, (b) 0.2 M, (c) 0.3 M, and (e) 0.5 M ion concentrations.

mol/L) is the equilibrium concentration of the ion in the solution.

3. RESULTS AND DISCUSSION

3.1. Structural Properties of Pb(II) Metal Ion. Figure 2 presents the normalized density distributions of lead (Pb^{2+}) ions as a function of distance from the graphene based materials in the aqueous solutions. Figure 2a displays the behavior of Pb^{2+} ions at 0.1 M solution. The formation of layers near the surface is clearly evident for all the systems considered in this work. The density of the Pb^{2+} ion is highest within the first contact layer, which subsequently decreases with increasing distance from the surface. The oscillation of the density is progressively damped out until the value of the bulk solution is recovered at around 15 Å, within three layers from the surface. The density of the peaks increases with modification of GS with PAMAM. The density peaks of Pb^{2+} ions on the dendrimer grafted GS surface are 2−3 orders higher than those of the bare GS, depending on the terminal groups of PAMAM. The Pb^{2+} ions interact favorably with the carboxyl, hydroxyl, and amide terminal groups of the dendrimer molecule grafted on the GS, leading to better adsorption characteristics than the bare GS surface for Pb^{2+}. In comparison with the dendrimer molecule with $-NH_2$ and −OH terminal groups, $-COO^-$, the terminal group considerably increases the metal ion near the surface as is evident from the enhanced peaks of the first layer. The effect is more pronounced at a lower concentration, which is evident from the pronounced peak heights and distinct four layers on the surface as seen in Figure 2a. This strongly indicates that the carboxyl terminal groups of the dendrimer molecules attract the metal ions near the GS surface relatively more than the other terminal groups of the dendrimer molecule. Therefore, the GS-PAMAM-COO^- surface displayed significantly higher Pb^{2+} ion adsorption capacity compared to the GS-PAMAM and GS-PAMAM-OH surfaces. The adsorption behavior is more or less similar to an increase in the salt concentration as seen in Figure 2b−d.

Figure 3 presents the density profiles of lead ions on the bare GO and dendrimer grafted on the GO surfaces. The first peaks of the density profiles for bare GO and GO grafted with dendrimer are substantially pronounced compared to that of the bare GS and GS grafted with dendrimer, which is much more evident at lower concentrations. In comparison with GS and dendimer grafted GS surfaces, the first layer slightly changes its positions (from 5 to 5.2 Å) because of functional groups on the GO surface. However, the peak height of the density profile is considerably increased. This shows that the GO and GO-PAMAM surfaces allow a relatively greater number of metal ions nearer the surface compared to the GS and PAMAM grafted GS surfaces. The peak height of the density profile of metal ion is different for different terminal groups ($-NH_2$, $-COO^-$, and −OH) indicative of the differences in their affinity toward the metal ions. Similar to the case for GS surfaces, for all salt concentrations, the GO-PAMAM-COO^- surface shows better Pb^{2+} ion adsorption capacity than the other three surfaces, which is evident from the

DOI: 10.1021/acs.jpca.7b09766
J. Phys. Chem. A 2017, 121, 9320−9329

larger peak heights as displayed in Figure 3. At higher concentrations, 0.2, 0.3, and 0.5 M (see Figure 3b–d), the number of peaks increases indicating that the lead ions form two or three coordination shells nearer the surfaces within 20 Å. This also shows that more lead ions are nearer the GO surface grafted with dendrimer containing carboxyl, hydroxyl, and amide terminals groups. Moreover, the density of lead ions is much higher near the GO-PAMAM-COO^- surface; this suggests that the first layer can accommodate more Pb^{2+} ions. Increasing the salt concentration in the ionic solutions will affect the density profiles of metal ions near the bare GO and dendrimer grafted GO surfaces. The excess carboxyl and hydroxyl terminal groups of the dendrimer molecule attract the opposite ionic species (Pb^{2+} ion), promoting the formation of second and third peaks near the surface with increasing Pb^{2+} ion concentration. In general, for all the salt concentrations, the first peak height of the normalized density profile of Pb^{2+} ion nearer the GS and GO surfaces, grafted with the dendrimer molecule containing carboxyl, hydroxyl, and amide terminal groups, shows substantially pronounced peaks compared to the bare GS and bare GO surfaces. Thus, it is clear that dendrimer enhances the adsorption capacity of the base material. For example, at 0.5 M, the numbers of ions adsorbed by GO-PAMAM, GO, GS-PAMAM, and GS are 57, 44, 33, and 28, respectively, clearly indicative of a strong PAMAM effect even at high salt concentrations. On the basis of the above analysis, the order of Pb^{2+} ion adsorption capacity on the eight different surfaces are GO-PAMAM-COO^- > GO-PAMAM-OH > GO-PAMAM > GO > GS-PAMAM-COO^- > GS-PAMAM-OH > GS-PAMAM > GS. This behavior is explained by the PMF values of metal ion on the eight different surfaces in a later section.

3.2. Adsorption Isotherms. In order to ascertain the adsorption capacity of different material surfaces used in this work, we plot adsorption amount of metal ion as a function of concentration. The adsorption capacity is based on the number of metal ions adsorbed within the first coordination shell of the axial density profiles. q_e (mg/g) is calculated by converting the total number of adsorbed metal ions into milligrams and finally dividing by the unit mass of the adsorbent. Figure 4 shows the adsorption isotherm of Pb^{2+} ion on the eight different surfaces. Table 2 summarizes the parameters obtained from the fitting of the adsorption isotherm to the Langmuir isotherm equation. The adsorption isotherms are fitted well (see Figure 4) using eq 7, with the correlation coefficient (R^2) close to 1, indicating that the adsorption of Pb^{2+} ion on the GS, GS-PAMAM, GS-PAMAM-COO^-, GS-PAMAM-OH, GO, and GO–PAMAM, GO-PAMAM-COO^-, and GO-PAMAM-OH surfaces follows the Langmuir model. The maximum adsorption capacities of Pb^{2+} ion on different surfaces calculated from the Langmuir isotherm equation follow the order GO-PAMAM-COO^- > GO-PAMAM-OH> GO-PAMAM > GO > GS-PAMAM-COO^- > GS-PAMAM-OH > GS-PAMAM > GS. The adsorption of Pb^{2+} ions on the GO-PAMAM-COO^- surface is significantly more than that on the other surfaces for all five concentrations considered in this work. The highest monolayer adsorption capacities for Pb^{2+} ions on the GO-PAMAM-COO^-, GO-PAMAM-OH, GO-PAMAM, and GO surfaces are found to be 1523.1, 1224.6, 1100.3, and 1043.93 mg/g, respectively. The monolayer adsorption capacities for Pb^{2+} ions on the GS-PAMAM-COO^-, GS-PAMAM-OH, GS-PAMAM, and GS surfaces are found to be 1050.1, 975.33, 862.4, and 795.33 mg/g, respectively. Recent experimental work studied

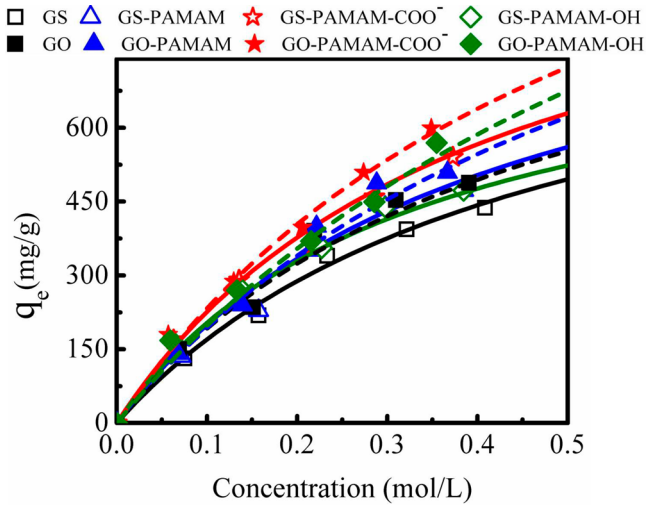

Figure 4. Langmuir adsorption isotherm showing the variation of total amount of Pb^{2+} ion adsorbed (q_e) onto different surfaces. Open symbols for different terminal groups ($-NH_2$, $-COO^-$, and $-OH$) of dendrimer grafted to GS surface and filled symbols for different terminal groups ($-NH_2$, $-COO^-$, and $-OH$) of dendrimer grafted to GO surface.

Table 2. Parameters of the Langmuir Isotherm Fitted to the Adsorption of Pb^{2+} Ions for Different Surfaces

	estimated Langmuir isotherm parameters	
surface	q_{max} (mg/g)	K
GS	795.33	0.3972
GS-PAMAM	862.4	1.157
GS-PAMAM-COO^-	1050.1	6.737
GS-PMAMA-OH	975.33	0.6109
GO	1043.9	1.554
GO-PAMAM	1100.3	1.946
GO-PAMAM-COO^-	1523.1	2.306
GO-PAMAM–OH	1224.6	1.63

the removal of heavy metal ions from aqueous solutions using GO-PAMAM adsorbent. The maximum adsorption capacity of GO-PAMAM for Pb^{2+} ion is found to be 568.18 mg/g at around 6 mmol/L. The maximum adsorption capacity of Pb^{2+} ion on the GO-PAMAM-COO^- surface, calculated from this work, is ∼62% higher than that from the experimental work. It should be noted that the pH of most of the wastewater streams is 6.0, whereas we have performed simulations for the neutral system at a pH of 7. Nevertheless, qualitatively the experimental findings of the order of adsorption of Pb^{2+} metal ion on the different surfaces GO-PAMAM > GO > GS are akin to those seen in this work.[37]

3.3. Diffusion Coefficient and Occupation Time Distribution Function. We have shown that PAMAM dendrimer increases the adsorption of the lead ion. Furthermore, with a suitable terminal group (COO^-) on the dendrimer, the adsorption amount can be significantly increased. In this section, we discuss the mobility and occupation time of the Pb^{2+} ions near the surface. To this end, we evaluate the in-plane mean square displacement (MSD) using eq 5, and use eq 6 to calculate the in-plane self-diffusion coefficient (D_{II}) along the plane of the substrate. Figure 5a presents the D_{II} values as a function of concentration for different surfaces. The results show that the in-plane

DOI: 10.1021/acs.jpca.7b09766
J. Phys. Chem. A 2017, 121, 9320–9329

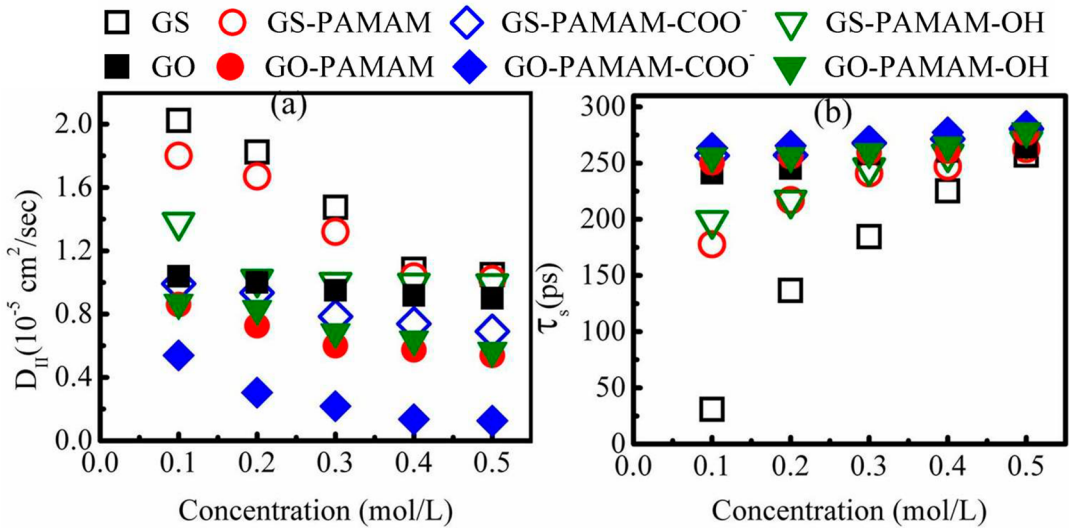

Figure 5. (a) Diffusion coefficients of Pb^{2+} ions nearer to the four different surfaces as a function of concentration. (b) Residence time of Pb^{2+} ions nearer to the four different surfaces as a function of concentration.

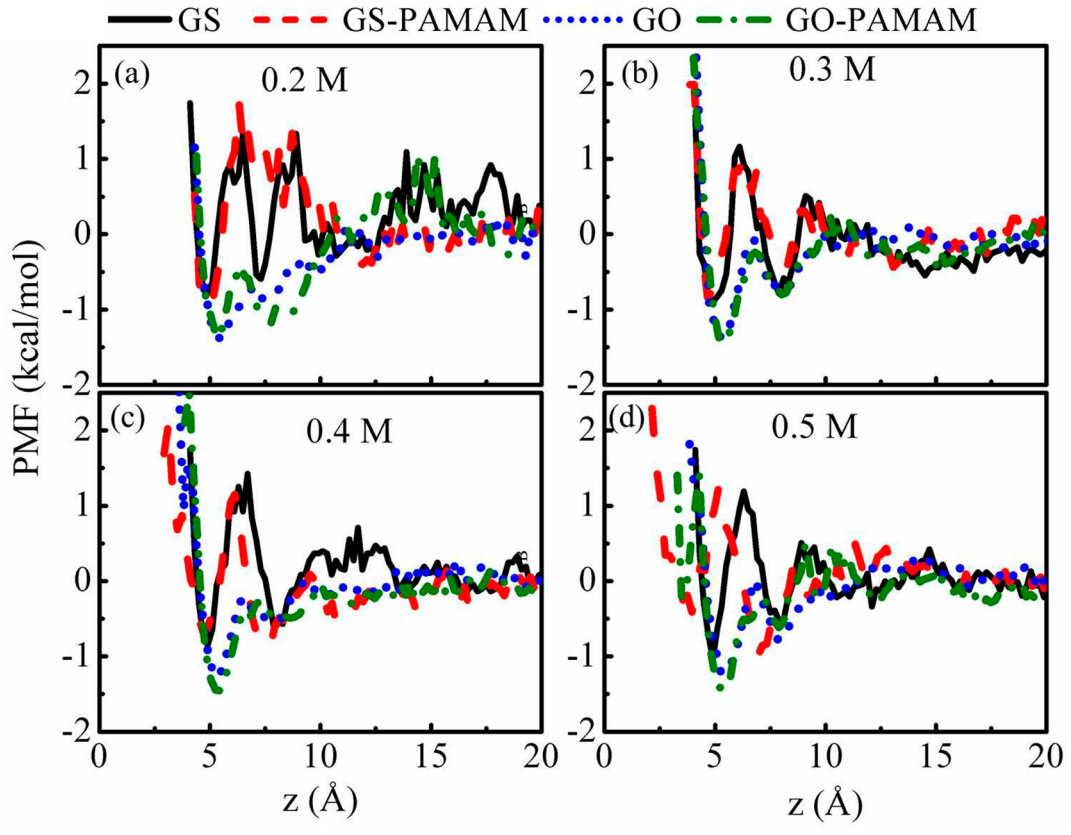

Figure 6. PMF profiles derived from average normalized densities of the Pb^{2+} ions in the presence of four different surfaces: (a) 0.2 M, (b) 0.3 M, (c) 0.4 M, (d) 0.5 M.

diffusion coefficient for Pb^{2+} ions near the different surfaces decreases with increasing metal ion concentration for eight different surfaces. The lower diffusion coefficient indicates a stronger affinity of the Pb^{2+} near the surfaces. The diffusion coefficient of Pb^{2+} ion is larger, almost at all concentrations, in the presence of the GS surface compared to the other surfaces. On the contrary, the diffusion coefficient values for Pb^{2+} ions in the presence of the GO-PAMAM-COO^- surface are smaller compared to those for GO, GO-PAMAM-OH, GS-PAMAM, GS-PAMAM-OH, and GS surfaces at all concentrations. This clearly indicates that the GO-PAMAM-COO^- surface has a stronger affinity for the metal ions among all the systems considered in this paper, and is thus a better adsorbent.

In addition to the in-plane diffusion coefficient, the occupation time distribution function $R(t)$ is also calculated to understand the residence time (τ_s) of Pb^{2+} ions on different surfaces, using eqs 3 and 4. Figure 5b represents the residence time of Pb^{2+} ions for eight different surfaces with increasing

DOI: 10.1021/acs.jpca.7b09766
J. Phys. Chem. A 2017, 121, 9320−9329

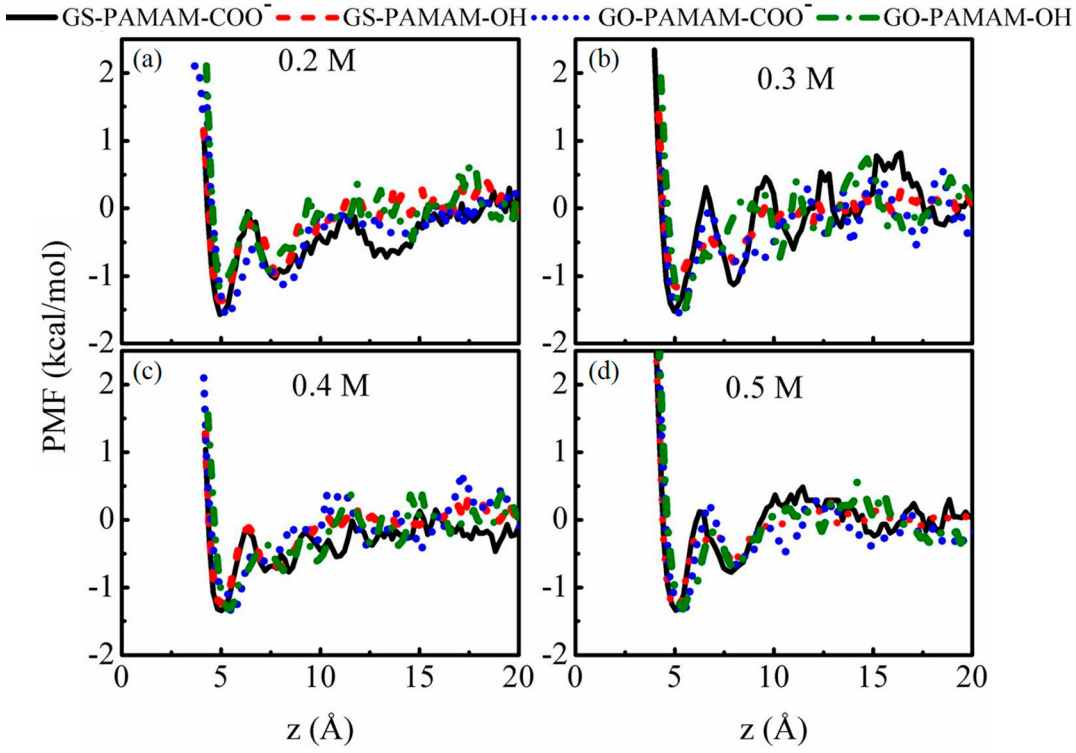

Figure 7. PMF profiles derived from average normalized densities of the Pb^{2+} ions in the presence of four different functional surfaces: (a) 0.2 M, (b) 0.3 M, (c) 0.4 M, (d) 0.5 M.

metal ion concentration. Similar to the behavior seen for the diffusivity values, the residence time of Pb^{2+} ions in the presence of GS is typically lowest among all the surfaces. On the contrary, the residence time of Pb^{2+} ions on the GO-PAMAM-COO^- surface is highest compared to those on other surfaces. Nevertheless, the salt concentration increases the residence time of the ions, and the effect is dramatic for the GS surface. The above behavior is in line with the observed diffusion values. The Pb^{2+} ion has a high residence time in the presence of the GO-PAMAM-COO^- surface compared to the GO, GO-PAMAM, GO-PAMAM-OH, GS-PAMAM-COO^-, GS-PAMAM-OH, GS-PAMAM, and GS surfaces. The lower diffusion coefficient and higher value of residence time of the Pb^{2+} ion further corroborate that it has a higher affinity for adsorption on the GO-PAMAM-COO^- surface. The larger value of residence time of the metal ion represents a greater affinity toward the GO-PAMAM-COO^- surface than the other seven surfaces. The in-plane diffusivity of the metal ion decreases with increasing metal ion concentration, respectively, in the following order: GO-PAMAM-COO^- < GO-PAMAM−OH < GO-PAMAM < GO < GS-PAMAM-COO^- < GS-PAMAM-OH < GS-PAMAM < GS surfaces. On the contrary, as expected, the residence time of the metal ion increases with increasing metal ion concentration follows the order: GO-PAMAM-COO^- > GO-PAMAM−OH> GO-PAMAM > GO> GS-PAMAM-COO^- > GS-PAMAM-OH > GS-PAMAM > GS surfaces.

We have also calculated the residence time of the water molecules when they are in the first solvation shell of the cation in the bulk phase and near the GO surface (monolayer). Figure S1, Supporting Information, shows an illustration of the adsorption of Pb^{2+} to the dendrimer's terminal groups. Figure S1(a) provides structures of the water molecules around the ion within the monolayer at the GO surface and away from the GO surface. The Pb^{2+} metal ions are partially solvated by water when they are in contact with the surface. On the other hand, the Pb^{2+} metal ions are fully solvated in the water reservoir, i.e., away from the surface. Figure S2, Supporting Information, shows the decay of residence time of water molecules in the first hydration shell of the Pb^{2+} ion for all the concentrations. The residence time of water molecules in the first hydration shell of various Pb^{2+} ions is around 2 times longer near the GO surface compared to that in the bulk phase, as evident from Table S1, Supporting Information. Furthermore, residence time increases with increasing concentration.

3.4. Potential of Mean Force. In order to understand the interaction behavior of the metal ion on different surfaces considered in this work, we evaluate the potential of mean force using the following expression:

$$A(z) = -k_B T \ln\left(\frac{\rho_{Pb}(z)}{\rho_{Pb}(\text{bulk})}\right)$$

Figure 6 illustrates the PMF profiles of the Pb^{2+} ions in the presence of different surfaces. In the case of 0.2 M (Figure 6a), the PMF value for Pb^{2+} ion on the GO-PAMAM surface (i.e., for contact layer) is −1.4 kcal/mol, which is much lower than the other three surfaces (GO, GS, and GS-PAMAM). The PMF profiles of Pb^{2+} with four different surfaces at 0.3 and 0.4 M concentration are shown in Figure 6b,c, respectively. At 0.3 and 0.4 M concentration, the PMF values for Pb^{2+} ions with GO-PAMAM surface are −1.4 and −1.6 kcal/mol, respectively. At 0.5 M the PMF values of the four different surfaces GO-PAMAM, GO, GS, and GS-PAMAM are −1.8, −1.4, −1.0, and −1.0 kcal/mol, respectively. It is evident from the above analysis that the PMF value of the ion reduces with an increase in the salt concentration. The lower free energy values indicate favorable adsorption of metal ions on the surface. It can be seen

DOI: 10.1021/acs.jpca.7b09766
J. Phys. Chem. A 2017, 121, 9320−9329

that PAMAM provides a favorable environment for Pb^{2+} ions to get adsorbed on the surface. This is clear from the lower PMF value for PAMAM grafted surfaces against the bare surface. The lower energy barrier of the metal ion is observed near the GO-PAMAM compared to the GS-PAMAM surface. In addition, GO is a relatively more preferred surface for the metal ion, as evident from the lower PMF value of GO compared to that for the GS surface (see Figure 6a). However, the sensitivity of the base surface (i.e., GO against GS) slightly reduces with an increase in the concentration as indicated by the decrease in the difference between the PMF values between the bare GS and the bare GO (see Figure 6a,d).

In addition to GS-PAMAM and GO-PAMAM, we also studied the effect of different terminal groups ($-COO^-$ and $-OH$) of dendrimer grafted GS and GO surfaces on the PMF of metal ions. Figure 7 shows the PMF profiles of the Pb^{2+} ion using carboxyl and hydroxyl terminal groups of dendrimer grafted on GS and GO surfaces. At 0.2 and 0.3 M concentrations, the PMF value for the Pb^{2+} ion is 1.9 kcal/mol for the GO-PAMAM-COO^- surface, which is much higher than that seen for the GS (0.8 kcal/mol) and GS-PAMAM (0.85 kcal/mol) surfaces. This is an indication of relative differences in the effective interactions of the ion with different substrates, which is in line with the residence time and slow diffusion values of the metal ion on the GO-PAMAM-COO^- surface. This, in particular, elucidates the effect of the carboxyl group on the adsorption and retention of the metal ions from an aqueous phase. Another important aspect in the adsorption of the metal ion on the surface is the free energy barrier, which the metal ions must overcome to get onto the surfaces. The energy barriers of Pb^{2+} ion, closer to the eight different surfaces, follow the order GO-PAMAM-COO^- < GO-PAMAM-OH < GO-PAMAM-OH < GO < GS-PAMAM-COO^- < GS-PAMAM-OH < GS-PAMAM < GS.

Figure 7 clearly displays that the Pb^{2+} ion faces a lower energy barrier (~0.5 kcal/mol) closer to the surfaces for dendrimer grafted on the GO surfaces, for all salt concentrations. This is due to the relatively greater number of carboxyl and hydroxyl terminal groups of the dendrimer molecule that cause a substantially lower energy barrier for the Pb^{2+} ions to approach the GO and GS surfaces. Contrary to that, the energy barriers of Pb^{2+} ion in the presence of bare GS and dendrimer grafted on the GS surfaces (GS-PAMAM) are significantly higher ~2.5 kcal/mol. It is evident from the above discussion that the carboxyl terminal groups of dendrimer grafted on the GS and GO surfaces display significantly smaller energy barriers and higher PMF values for Pb^{2+} ion, which indicates a promising material for the removal of Pb^{2+} ions.

4. CONCLUSION

We have used molecular dynamics tools to study the separation of Pb^{2+} metal ions from aqueous solutions using bare GS, bare GO, and PAMAM dendrimer grafted GS and GO surfaces. The adsorption behavior is well-described by the Langmuir isotherm model. The adsorption capacity of Pb^{2+} ions on the dendrimer grafted on the GO surface is significantly more than those of the bare GO, bare GS, and dendrimer grafted GS surfaces for five concentrations. The adsorption mechanism of metal ions on the eight different surfaces is discussed with the help of microscopic interactions between the metal ion and solid surfaces. We have also examined the self-diffusion coefficient and residence time of Pb^{2+} ions near the surfaces. Interestingly, we find that the interaction between the Pb^{2+} ion and dendrimer plays a significant role in enhancing their association with the dendrimer grafted surfaces. The results show that adsorption capacity of the Pb^{2+} ion is improved significantly using carboxyl terminal groups of dendrimer grafted on a graphene oxide surface. The following order of adsorption capacity of Pb^{2+} ion is found, GO-PAMAM-COO^- > GO-PAMAM-OH > GO-PAMAM > GO > GS-PAMAM-COO^- > GS-PAMAM-OH > GS-PAMAM > GS, which is well supported by the PMF calculations.

■ ASSOCIATED CONTENT

Supporting Information

The Supporting Information is available free of charge on the ACS Publications website at DOI: 10.1021/acs.jpca.7b09766.

Snapshots of water structure on the GO surface and away from the GO surface, illustration of ion adsorption on dendrimer grafted GO surface, and residence times of water molecules near the GO surface and in the bulk phase (PDF)

■ AUTHOR INFORMATION

Corresponding Author

*E-mail: jayantks@iitk.ac.in. Phone: 91-512- 259 6141. Fax: 91-512-259 0104.

ORCID

Jayant K. Singh: 0000-0001-8056-2115

Notes

The authors declare no competing financial interest.

■ ACKNOWLEDGMENTS

This is funded by the Department of Atomic Energy (sanctioned number: 36(1)/14/02/2015-BRNS/100). V.V. and M.N.D.S.C. acknowledged the financial support from Fundação para a Ciência e a Tecnologia (FCT/MEC) through national funds, and cofinanced by the European Union (FEDER funds) under the Partnership Agreement PT2020, through projects UID/QUI/50006/2013, POCI/01/0145/FEDER/007265, and NORTE-01-0145-FEDER-000011 (LAQV@REQUIMTE).

■ REFERENCES

(1) Nriagu, J. O.; Pacyna, J. M. Quantitative Assessment of Worldwide Contamination of Air, Water and Soils by Trace Metals. *Nature* **1988**, *333*, 134−139.

(2) Yao, T.; Cui, T.; Wu, J.; Chen, Q.; Lu, S.; Sun, K. Preparation of Hierarchical Porous Polypyrrole Nanoclusters and their Application for Removal of Cr(VI) ions in Aqueous Solution. *Polym. Chem.* **2011**, *2*, 2893−2899.

(3) Kadirvelu, K.; Thamaraiselvi, K.; Namasivayam, C. Removal of Heavy Metals from Industrial Wastewaters by Adsorption onto Activated Carbon Prepared from an Agricultural Solid Waste. *Bioresour. Technol.* **2001**, *76*, 63−65.

(4) Aman, T.; Kazi, A. A.; Sabri, M. U.; Bano, Q. Potato Peels as Solid Waste for the Removal of Heavy Metal Copper(II) from Waste Water/Industrial Effluent. *Colloids Surf., B* **2008**, *63*, 116−121.

(5) Jiang, Y.; Pang, H.; Liao, B. Removal of Copper(II) Ions from Aqueous Solution by Modified Bagasse. *J. Hazard. Mater.* **2009**, *164*, 1−9.

(6) Babel, S.; Kurniawan, T. A. Cr(VI) Removal from Synthetic Wastewater using Coconut Shell Charcoal and Commercial Activated Carbon Modified with Oxidizing Agents and/or Chitosan. *Chemosphere* **2004**, *54*, 951−967.

DOI: 10.1021/acs.jpca.7b09766
J. Phys. Chem. A 2017, 121, 9320−9329

(7) Samiey, B.; Cheng, C.-H.; Wu, J. Organic-Inorganic Hybrid Polymers as Adsorbents for Removal of Heavy Metal Ions from Solutions: A Review. *Materials* **2014**, *7*, 673−726.
(8) Netzer, A.; Hughes, D. E. Adsorption of Copper, Lead and Cobalt by Activated Carbon. *Water Res.* **1984**, *18*, 927−933.
(9) Ray, P. Z.; Shipley, H. J. Inorganic Nano-adsorbents for the Removal of Heavy Metals and Arsenic: A Review. *RSC Adv.* **2015**, *5*, 29885−29907.
(10) Gharabaghi, M.; Irannajad, M.; Azadmehr, A. R. Selective Sulphide Precipitation of Heavy Metals from Acidic Polymetallic Aqueous Solution by Thioacetamide. *Ind. Eng. Chem. Res.* **2012**, *51*, 954−963.
(11) Khan, A. A.; Paquiza, L. Characterization and Ion-exchange Behavior of Thermally Stable Nano-composite Polyaniline Zirconium Titanium Phosphate: Its Analytical Application in Separation of Toxic Metals. *Desalination* **2011**, *265*, 242−254.
(12) Yanagisawa, H.; Matsumoto, Y.; Machida, M. Adsorption of Zn(II) and Cd(II) Ions onto Magnesium and Activated Carbon Composite in Aqueous Solution. *Appl. Surf. Sci.* **2010**, *256*, 1619−1623.
(13) Mohsen-Nia, M.; Montazeri, P.; Modarress, H. Removal of Cu^{2+} and Ni^{2+} from Wastewater with a Chelating Agent and Reverse Osmosis Processes. *Desalination* **2007**, *217*, 276−281.
(14) Marjani, A.; Shirazian, S. Simulation of Heavy Metal Extraction in Membrane Contactors Using Computational Fluid Dynamics. *Desalination* **2011**, *281*, 422−428.
(15) Fonseca, B.; Figueiredo, H.; Rodrigues, J.; Queiroz, A.; Tavares, T. Mobility of Cr, Pb, Cd, Cu and Zn in a Loamy Sand Soil: A Comparative Study. *Geoderma* **2011**, *164*, 232−237.
(16) Tan, X.; Fang, M.; Chen, C.; Yu, S.; Wang, X. Counterion Effects of Nickel and Sodium Dodecylbenzene Sulfonate Adsorption to Multiwalled Carbon Nanotubes in Aqueous Solution. *Carbon* **2008**, *46*, 1741−1750.
(17) Tan, X.; Fan, Q.; Wang, X.; Grambow, B. Eu(III) Sorption to TiO2 (Anatase and Rutile): Batch, XPS, and EXAFS Studies. *Environ. Sci. Technol.* **2009**, *43*, 3115−3121.
(18) Long, R. Q.; Yang, R. T. Carbon Nanotubes as Superior Sorbent for Dioxin Removal. *J. Am. Chem. Soc.* **2001**, *123*, 2058−2059.
(19) Wang, X.; Lu, J.; Xing, B. Sorption of Organic Contaminants by Carbon Nanotubes: Influence of Adsorbed Organic Matter. *Environ. Sci. Technol.* **2008**, *42*, 3207−3212.
(20) Yang, S.; Hu, J.; Chen, C.; Shao, D.; Wang, X. Mutual Effects of Pb(II) and Humic Acid Adsorption on Multiwalled Carbon Nanotubes/Polyacrylamide Composites from Aqueous Solutions. *Environ. Sci. Technol.* **2011**, *45*, 3621−3627.
(21) Chandra, V.; Park, J.; Chun, Y.; Lee, J. W.; Hwang, I.-C.; Kim, K. S. Water-Dispersible Magnetite-Reduced Graphene Oxide Composites for Arsenic Removal. *ACS Nano* **2010**, *4*, 3979−3986.
(22) Chandra, V.; Kim, K. S. Highly Selective Adsorption of Hg^{2+} by a Polypyrrole-Reduced Graphene Oxide Composite. *Chem. Commun.* **2011**, *47*, 3942−3944.
(23) Zhao, G.; Jiang, L.; He, Y.; Li, J.; Dong, H.; Wang, X.; Hu, W. Sulfonated Graphene for Persistent Aromatic Pollutant Management. *Adv. Mater.* **2011**, *23*, 3959−3963.
(24) Zhang, N.; Qiu, H.; Si, Y.; Wang, W.; Gao, J. Fabrication of Highly Porous Biodegradable Monoliths Strengthened by Graphene Oxide and Their Adsorption of Metal Ions. *Carbon* **2011**, *49*, 827−837.
(25) Mi, X.; Huang, G.; Xie, W.; Wang, W.; Liu, Y.; Gao, J. Preparation of Graphene Oxide Aerogel and Its Adsorption for Cu^{2+} Ions. *Carbon* **2012**, *50*, 4856−4864.
(26) Machida, M.; Mochimaru, T.; Tatsumoto, H. Lead(II) Adsorption onto the Graphene Layer of Carbonaceous Materials in Aqueous Solution. *Carbon* **2006**, *44*, 2681−2688.
(27) Sreeprasad, T. S.; Maliyekkal, S. M.; Lisha, K. P.; Pradeep, T. Reduced Graphene Oxide-Metal/Metal Oxide Composites: Facile Synthesis and Application in Water Purification. *J. Hazard. Mater.* **2011**, *186*, 921−931.
(28) Liu, L.; Li, C.; Bao, C.; Jia, Q.; Xiao, P.; Liu, X.; Zhang, Q. Preparation and Characterization of Chitosan/Graphene Oxide Composites for the Adsorption of Au(III) and Pd(II). *Talanta* **2012**, *93*, 350−357.
(29) Hao, L.; Song, H.; Zhang, L.; Wan, X.; Tang, Y.; Lv, Y. SiO2/Graphene Composite for Highly Selective Adsorption of Pb(II) Ion. *J. Colloid Interface Sci.* **2012**, *369*, 381−387.
(30) Deng, X.; Lü, L.; Li, H.; Luo, F. The Adsorption Properties of Pb(II) and Cd(II) on Functionalized Graphene Prepared by Electrolysis Method. *J. Hazard. Mater.* **2010**, *183*, 923−930.
(31) Li, Z.; Chen, F.; Yuan, L.; Liu, Y.; Zhao, Y.; Chai, Z.; Shi, W. Uranium(VI) Adsorption on Graphene Oxide Nanosheets from Aqueous Solutions. *Chem. Eng. J.* **2012**, *210*, 539−546.
(32) Anitha, K.; Namsani, S.; Singh, J. K. Removal of Heavy Metal Ions Using a Functionalized Single-Walled Carbon Nanotube: A Molecular Dynamics Study. *J. Phys. Chem. A* **2015**, *119*, 8349−8358.
(33) Kommu, A.; Namsani, S.; Singh, J. K. Removal of Heavy Metal Ions Using Functionalized Graphene Membranes: A Molecular Dynamics Study. *RSC Adv.* **2016**, *6*, 63190−63199.
(34) Tomalia, D. A.; Baker, H.; Dewald, J.; Hall, M.; Kallos, G.; Martin, S.; Roeck, J.; Ryder, J.; Smith, P. A New Class of Polymers: Starburst-Dendritic Macromolecules. *Polym. J.* **1985**, *17*, 117−132.
(35) Tomalia, D. A.; Baker, H.; Dewald, J.; Hall, M.; Kallos, G.; Martin, S.; Roeck, J.; Ryder, J.; Smith, P. Dendritic Macromolecules: Synthesis of Starburst Dendrimers. *Macromolecules* **1986**, *19*, 2466−2468.
(36) Yuan, Y.; Zhang, G.; Li, Y.; Zhang, G.; Zhang, F.; Fan, X. Poly(amidoamine) Modified Graphene Oxide as an Efficient Adsorbent for Heavy Metal Ions. *Polym. Chem.* **2013**, *4*, 2164−2167.
(37) Zhang, F.; Wang, B.; He, S.; Man, R. Preparation of Graphene-Oxide/Polyamidoamine Dendrimers and Their Adsorption Properties toward Some Heavy Metal Ions. *J. Chem. Eng. Data* **2014**, *59*, 1719−1726.
(38) Case, D. A.; Darden, T. A.; Cheatham, I. T.E.; Simmerling, C. L.; Wang, J.; Duke, R. E.; Luo, R.; Walker, R. C.; Zhang, W.; Merz, K. M.; et al. *AMBER12*; University of California: San Francisco, CA, 2012.
(39) Maingi, V.; Jain, V.; Bharatam, P. V.; Maiti, P. K. Dendrimer Building Toolkit: Model Building and Characterization of Various Dendrimer Architectures. *J. Comput. Chem.* **2012**, *33*, 1997−2011.
(40) Frisch, M. J.; Trucks, G. W.; Schlegel, H. B.; Scuseria, G. E.; Robb, M. A.; Cheeseman, J. R.; Montgomery, J. A., Jr.; Vreven, T.; Kudin, K. N.; Burant, J. C.; et al. *GAUSSIAN 03*; Gaussian Inc.: Pittsburgh, PA, 2003.
(41) Jorgensen, W. L.; Chandrasekhar, J.; Madura, J. D.; Impey, R. W.; Klein, M. L. Comparison of Simple Potential Functions for Simulating Liquid Water. *J. Chem. Phys.* **1983**, *79*, 926−935.
(42) Jorgensen, W. L.; Maxwell, D. S.; Tirado-Rives, J. Development and Testing of the OPLS All-Atom Force Field on Conformational Energetics and Properties of Organic Liquids. *J. Am. Chem. Soc.* **1996**, *118*, 11225−11236.
(43) Peng, Y.; Kaminski, G. A. Accurate Determination of Pyridine Poly(amidoamine) Dendrimer Absolute Binding Constants with the OPLS-AA Force Field and Direct Integration of Radial Distribution Functions. *J. Phys. Chem. B* **2005**, *109*, 15145−15149.
(44) Jiao, S.; Xu, Z. Selective Gas Diffusion in Graphene Oxides Membranes: A Molecular Dynamics Simulations Study. *ACS Appl. Mater. Interfaces* **2015**, *7*, 9052−9059.
(45) Tummala, N. R.; Striolo, A. Role of Counterion Condensation in the Self-Assembly of SDS Surfactants at the Water-Graphite Interface. *J. Phys. Chem. B* **2008**, *112*, 1987−2000.
(46) Shih, C.-J.; Lin, S.; Sharma, R.; Strano, M. S.; Blankschtein, D. Understanding the pH-Dependent Behavior of Graphene Oxide Aqueous Solutions: A Comparative Experimental and Molecular Dynamics Simulation Study. *Langmuir* **2012**, *28*, 235−241.
(47) Plimpton, S. Fast Parallel Algorithms for Short-Range Molecular Dynamics. *J. Comput. Phys.* **1995**, *117*, 1−19.
(48) Martínez, L.; Andrade, R.; Birgin, E. G.; Martínez, J. M. PACKMOL: A Package for Building Initial Configurations for

DOI: 10.1021/acs.jpca.7b09766
J. Phys. Chem. A 2017, 121, 9320−9329

Molecular Dynamics Simulations. *J. Comput. Chem.* **2009**, *30*, 2157−2164.
(49) Hoover, W. G. Canonical Dynamics: Equilibrium Phase-Space Distributions. *Phys. Rev. A: At., Mol., Opt. Phys.* **1985**, *31*, 1695−1697.
(50) Nosé, S. A Unified Formulation of the Constant Temperature Molecular Dynamics Methods. *J. Chem. Phys.* **1984**, *81*, 511−519.

DOI: 10.1021/acs.jpca.7b09766
J. Phys. Chem. A 2017, 121, 9320−9329